

Bifurcation theory explains waveform variability in a congenital eye movement disorder

Andrea K. Barreiro · Jared C. Bronski ·
Thomas J. Anastasio

Received: 29 January 2008 / Revised: 25 June 2008 / Accepted: 9 July 2008 / Published online: 30 August 2008
© Springer Science + Business Media, LLC 2008

Abstract In dynamical systems, configurations that permit flexible control are also prone to undesirable behavior. We study a bilateral model of the oculomotor pre-motor network that conforms with the neuroanatomical constraint that brainstem neurons project to cerebellar Purkinje cells on both sides, but Purkinje cells project back to brainstem neurons on the same side only. Bifurcation analysis reveals that this network asymmetry enables flexible control by the cerebellum of brainstem network dynamics, but small changes in connection pattern or strength lead to behavior that is unstable, oscillatory, or both. The model produces the full range of waveform types associated with the hereditary eye movement disorder known as congenital nystagmus, and is consistent with findings linking the disorder with abnormal connectivity or limited plasticity in the cerebellum.

Keywords Congenital nystagmus · Infantile nystagmus · Oculomotor system · Neural integrator · Cerebellum · Mathematical model

Action Editor: G. Bard Ermentrout

A. K. Barreiro · J. C. Bronski
Department of Mathematics, University of Illinois
at Urbana-Champaign, 273 Altgeld Hall, 1409 Green Street,
Urbana, IL 61801, USA

T. J. Anastasio (✉)
Department of Molecular and Integrative Physiology,
Beckman Institute for Advanced Science and Technology,
University of Illinois at Urbana-Champaign,
405 North Mathews Avenue, Urbana, IL 61801, USA
e-mail: tja@uiuc.edu

1 Introduction

Congenital nystagmus (CN), now known also as infantile nystagmus, is a hereditary disorder characterized by uncontrollable eye movements that are oscillatory (pendular), unstable (jerk), or both (Maybodi 2003). Models of CN originally focused on the oculomotor integrator, a brainstem neural network that converts eye-velocity signals into the eye-position commands that are essential for eye-movement control (Robinson 1989). Brainstem integrator neurons collectively produce temporal integration by exerting positive feedback on each other (Robinson 1989). In integrator models, errors in tuning of positive feedback weights lead to instability but not to oscillation. Further, it was observed that oscillation could coexist with normal integrating function in CN patients (Dell'Osso et al. 1974), but models based on the integrator (Optican and Zee 1984) or the saccadic system (Akman et al. 2005) were unable to simulate this phenomenon. This led some researchers to suggest that oscillation in CN is due to increased delay in the smooth pursuit system (Jacobs and Dell'Osso 2004), leaving an abnormal integrator to blame for instability (Dell'Osso 1982).

A potential drawback of this view, in which CN has two separate causes that are segregated into different oculomotor subsystems, is that it does not account for the close pathophysiological relationship between the two basic forms of CN. The different forms can occur in different individuals in the same family, and even in the same individual at different eye positions (Dell'Osso et al. 1972, 1974; Dell'Osso and Daroff 1975; Yee et al. 1976). The observation that jerk and pendular CN can both occur in the same individual does not support the hypothesis that jerk nystagmus is an optimal

eye-movement strategy, employed by adults, that compensates for reduced, high-spatial-frequency visual contrast sensitivity, and that pendular CN is a non-optimal strategy employed by children with immature saccadic systems (Harris and Berry 2006). The close pathophysiological relationship between the two basic forms of CN suggests that they both arise from small changes occurring in the same subsystem. Here we provide an analysis of a network model of a single oculomotor subsystem that is consistent with neuroanatomy. The model produces the full range of waveform types observed in CN with only minor changes to its connection strengths.

2 Methods

Our analysis is based on a model of the neural integrator that includes the connections between the brainstem and the cerebellum. A schematic of the brainstem-cerebellar network is shown in Fig. 1. It is

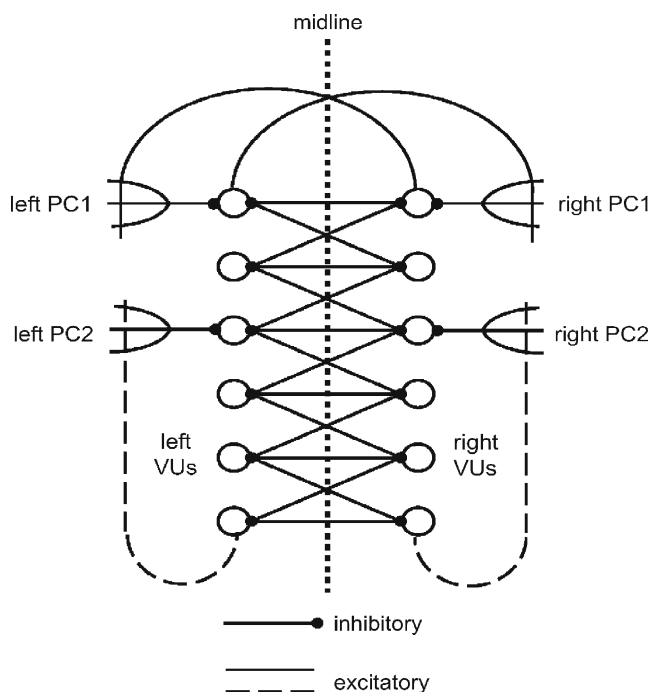


Fig. 1 Schematic diagram of the bilateral brainstem-cerebellar model. Circles and pitchforks represent brainstem integrator neurons (VUs) and cerebellar Purkinje cells (PCs), respectively. VUs project to each other contralaterally. PCs only project to VUs ipsilaterally, but VUs can project to PCs ipsilaterally (dashed connections) or contralaterally (solid connections). For clarity only a few of the VU–PC connections are shown

composed of elements representing neural types that are known to be essential for neural integration. The VUs represent neurons in the medial vestibular (MVN) and prepositus hypoglossi (NPH) nuclei in the brainstem. The PCs represent Purkinje cells in the floccular complex of the cerebellum. Lesions of these structures cause profound integrator deficits (Cannon and Robinson 1987; Zee et al. 1981; Chelazzi et al. 1990). With a normal, intact cerebellum, integrator time constant and gain are independently adjustable (Tiliket et al. 1994). The brainstem portion of the model is similar to previous models of the mammalian integrator in that VUs are arranged on either side of a bilateral network, and connected over the midline by reciprocal inhibition (Robinson 1989). The cerebellar connections conform to the neuroanatomic asymmetry by which the floccular complex receives input bilaterally from brainstem MVN/NPH neurons, but floccular Purkinje cells inhibit MVN/NPH neurons on the same (ipsilateral) side only (Büttner-Ennever 1988).

It is important to make a distinction between bilateral symmetry and network symmetry. The model we consider here is bilaterally symmetric because the VU-to-VU, VU-to-PC, and PC-to-VU connections are the same on both sides. We refer to a model as being network symmetric if the matrix representing the connections between units is symmetric across the main diagonal. This would correspond to the VU–PC connections being the same as the PC–VU connections. Most previous models of the neural integrator that lack PCs are both network and bilaterally symmetric (Robinson 1989). Systems having network symmetry are called self-adjoint in the mathematics literature, and it is well-known that such systems can not exhibit oscillation, but only exponential growth and decay. Our model is not network symmetric, since the VU–PC connections are very different from the PC–VU connections in the ways described above. As a result this model can exhibit more complicated dynamics than simple exponential growth and decay, including oscillation and high gain.

Networks have twelve VUs (six per side). They have only four PCs (two per side), and each PC contacts only one VU, to reflect the sparseness of innervation of MVN/NPH by the floccular complex (Babalian and Vidal 2000). We manipulate both PC–VU and VU–PC connection weights. Changing the weight of the single PC–VU connection of a PC is equivalent to scaling the weights of all of the VU connections to that PC by the same amount. Therefore we consider the ability to modify single PC–VU weights, or individual VU–PC

weights, as gross or fine control, respectively, and will argue that CN might result from abnormalities in cerebellar development or adaptive capability that limit plasticity to gross control of synaptic weights.

A recent study using a genetic algorithm found many “fit” configurations of the brainstem-cerebellar network model in which time constant and gain could be adjusted independently by changing only the PC–VU weights (Anastasio and Gad 2007). Here we show analytically that robust gain adjustment is possible only because of the lack of network symmetry (connections between VUs and PCs are asymmetric). This condition is necessary but not sufficient for normal function. Certain patterns of VU–PC connectivity can satisfy this condition but produce abnormal networks in which gain cannot be increased without introducing oscillation and/or instability.

We analyze two networks, one normal and one abnormal. The VU–PC connections for the normal network were set to an arbitrary pattern of ones and zeros (Table 1). We then found the abnormal network by making small changes to the pattern of VU–PC connections of the normal network (fewer than 17% of the VU–PC connections differ between the normal and abnormal networks). We assume that a normal cerebellum has developmental and/or adaptive fine control sufficient to establish a normal pattern of VU–PC connectivity, but an abnormal cerebellum does not. We further assume that both normal and abnormal networks are capable of gross control. Therefore in both networks the PC–VU weights vary, while the VU–PC weights are fixed.

Network element (unit) dynamics are first-order and linear. The firing rates of MVN/NPH neurons are linearly related to eye position and velocity above a threshold (Stahl and Simpson 1995). Cut-off of MVN/NPH neuron firing rates below threshold may account for eye-position dependent switching between different forms of CN (see Section 3). Denoting left and right side vestibular neurons by v_i^L and v_i^R respectively,

and similarly left and right side Purkinje cells by P_i^L and P_i^R , we have the following dynamical system:

$$\frac{dv_i^L}{dt} = \alpha \left(-v_i^L - \beta (v_{i+1}^R + v_i^R + v_{i-1}^R) - \rho_1 \delta_{i,k_1} P_1^L - \rho_2 \delta_{i,k_2} P_2^L \right) \tag{1}$$

$$\frac{dv_i^R}{dt} = \alpha \left(-v_i^R - \beta (v_{i+1}^L + v_i^L + v_{i-1}^L) - \rho_1 \delta_{i,k_1} P_1^R - \rho_2 \delta_{i,k_2} P_2^R \right) \tag{2}$$

$$\frac{dP_i^L}{dt} = \alpha \left(-P_i^L + \vec{w}_i^I \cdot \vec{v}^L + \vec{w}_i^C \cdot \vec{v}^R \right) \tag{3}$$

$$\frac{dP_i^R}{dt} = \alpha \left(-P_i^R + \vec{w}_i^I \cdot \vec{v}^R + \vec{w}_i^C \cdot \vec{v}^L \right). \tag{4}$$

Here $1/\alpha = 5\text{ms}$ (Robinson 1989) is the time-constant of a single neuron, giving $\alpha = 200\text{s}^{-1}$. The constant β is the weight of the reciprocally inhibitory connections between VUs. In the absence of the cerebellum the time-constant for the integrator is reduced from about 20s to about 1s in primates (Zee et al. 1981), and from about 2s to under 1s in rodents (Chelazzi et al. 1990). To demonstrate the robustness of the model, we choose β to give a time-constant for the integrator of 0.2s in the absence of PCs ($\beta = 0.348$). Taking a time-constant of 1s in the absence of PCs ($\beta = 0.355$) produces a model with qualitatively similar results. Vectors \vec{w}_i^I and \vec{w}_i^C are the ipsilateral and contralateral VU–PC weight vectors, and adjustable parameters ρ_1 and ρ_2 are the PC–VU weights of PCs 1 and 2. The Kronecker delta ($\delta_{i,j}$) is 1 when $i = j$ and 0 otherwise.

Because of bilateral symmetry the system decouples into common modes $\vec{v}^R = \vec{v}^L$ and push-pull modes $\vec{v}^R = -\vec{v}^L$. Because the dominant modes are all push-pull modes, and because push-pull modes are the most relevant to integrator function (Robinson 1989), we consider only these modes. In terms of the difference variables $\vec{v} = \vec{v}^R - \vec{v}^L$, $\vec{P} = \vec{P}^R - \vec{P}^L$ the system becomes

$$\frac{d\vec{V}}{dt} = \mathbf{M}\vec{V},$$

Table 1 VU–PC connections for the three networks simulated in this paper

Connection type	Normal	Abnormal/Cy. left	Cycloidal right
\vec{w}_1^I	[0, 1, 0, 0, 0, 1]	[0, 1, 0, 0, 0, 1]	[0, γ_1 , 0, 0, 0, 1]
\vec{w}_1^C	[1, 0, 1, 0, 1, 1]	[1, 0, 0, 0, 1, 1]	[1, 0, γ_2 , 0, 1, 1]
\vec{w}_2^I	[1, 0, 1, 1, 0, 1]	[1, 0, 0, 0, 1, 1]	[1, 0, 0, 0, 1, 1]
\vec{w}_2^C	[0, 1, 0, 0, 0, 1]	[0, 1, 0, 0, 0, 1]	[0, 1, 0, 0, γ_3 , 1]

“Normal” denotes the network whose phase space is shown in Fig. 2(a) and “abnormal” denotes the network whose phase space is shown in Fig. 2(b). To produce the cycloidal CN shown in Fig. 3(c), modest changes were made to the “abnormal” network to produce “cycloidal right”. Here $\gamma_{1,2,3} \approx 1.5, 0.5, 2.5$ respectively

where \mathbf{M} is a $(n + 2) \times (n + 2)$ matrix. Our experimental network is

$$\mathbf{M} = \alpha \left(\begin{array}{cccccc|cc} -1 + \beta & \beta & 0 & 0 & 0 & 0 & -\rho_1 & 0 \\ \beta & -1 + \beta & \beta & 0 & 0 & 0 & 0 & 0 \\ 0 & \beta & -1 + \beta & \beta & 0 & 0 & 0 & -\rho_2 \\ 0 & 0 & \beta & -1 + \beta & \beta & 0 & 0 & 0 \\ 0 & 0 & 0 & \beta & -1 + \beta & \beta & 0 & 0 \\ 0 & 0 & 0 & 0 & \beta & -1 + \beta & 0 & 0 \\ \hline & & \vec{w}_1 & & & & -1 & 0 \\ & & \vec{w}_2 & & & & 0 & -1 \end{array} \right) \tag{5}$$

where the new VU–PC coupling vectors are given by the difference between the ipsilateral and contralateral vectors, $\vec{w}_i = \vec{w}_i^I - \vec{w}_i^C$. Note the change in sign of β : in the difference variables the mutual inhibition between sides becomes an effective self-excitation.

Only the VUs receive input from outside the network. The input vector \vec{b} is set to excite left-side VUs and inhibit right-side VUs, thus providing a push-pull input to the VUs. The response of the network to arbitrary input signal $s(t)$ is:

$$\vec{V}(t) = \sum_i \vec{e}_i \frac{\vec{f}_i \cdot \vec{b}}{\vec{f}_i \cdot \vec{e}_i} \int_0^t e^{\lambda_i(t-t')} s(t') dt'$$

where we define right and left eigenvectors \vec{e}_i and \vec{f}_i by

$$\begin{aligned} \mathbf{M}\vec{e}_i &= \lambda_i \vec{e}_i \\ \mathbf{M}^T \vec{f}_i &= \lambda_i \vec{f}_i. \end{aligned}$$

The push–pull command to move the eyes is the sum of the VU responses on one side, minus the sum of the VU responses on the other side. Denoted by $c(t)$, this command is given by the inner product of \vec{V} with \vec{b} :

$$c(t) \equiv \vec{b} \cdot \vec{V}(t). \tag{6}$$

In the networks we examine, only a few modes dominate, with the rest contributing very brief transients. The gain of any mode i , and notably of the integrating mode, which is a real mode corresponding to a time constant of 20s, can be expressed in terms of the cosines of the angles between the input vector and the eigenvectors of that mode:

$$g = \frac{(\vec{b} \cdot \vec{e}_i)(\vec{f}_i \cdot \vec{b})}{(\vec{f}_i \cdot \vec{e}_i)(\vec{b} \cdot \vec{b})} = \frac{\cos(\theta_{be}) \cos(\theta_{bf})}{\cos(\theta_{ef})}$$

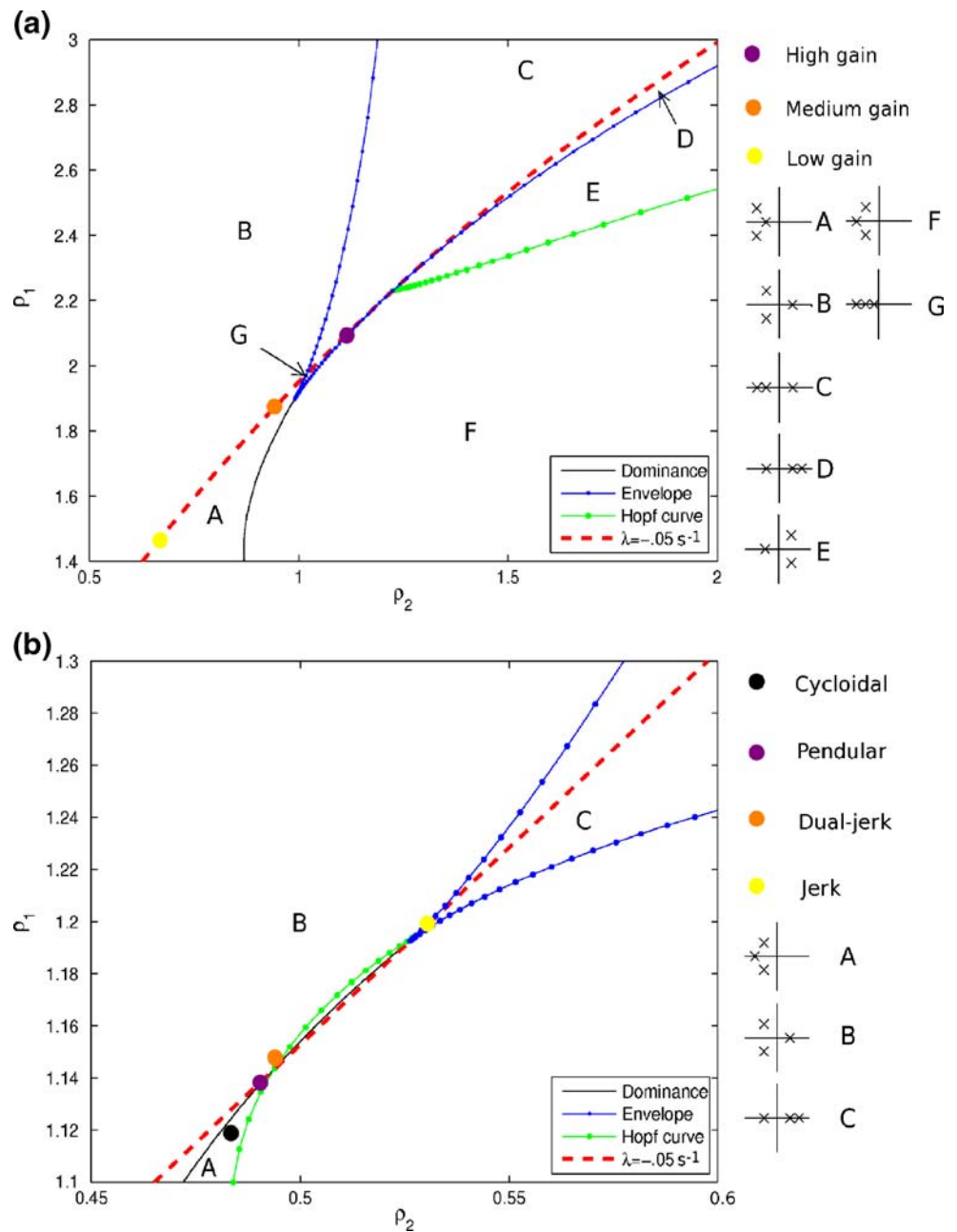
where $\cos(\theta_{be})$ is the cosine of the angle between \vec{b} and \vec{e}_i , and similarly for the other two angles. This

expression assumes that there is a single real dominant mode, an approximation which holds for most parameter values. For the numerical experiments presented here g reflects the overall gain of the system to within 3%.

We now note the following important fact: in the case where \mathbf{M} is self-adjoint (network symmetric), as in previous integrator models that omit the cerebellum (Robinson 1989), the left and right eigenvectors are the same, $\vec{e}_i = \vec{f}_i$, and $\cos(\theta_{ef}) = 1$. Thus gain for any single mode is at most one, and the amplitude of command $c(t)$, given by Eq. (6), is at most twelve. In the non-self-adjoint (network asymmetric) case, however, the denominator $\cos(\theta_{ef})$ can be arbitrarily close to zero, and thus gain can be made arbitrarily large. Further, since the denominator is small, relatively small changes in the left and the right eigenvectors can lead to large changes in gain (Anastasio and Gad 2007). This phenomenon is well known in applied mathematics (Embree and Trefethen 2001; Trefethen 1997). In non-self-adjoint systems the norm of the exponential $\|e^{t\mathbf{M}}\|$ can be much larger than might be predicted on the basis of the eigenvalues alone, because it is no longer determined solely by the eigenvalues but also involves geometric information about the eigenvectors (the angles between the left and right eigenvectors). We believe that the brainstem-cerebellar integrator exploits this mechanism as a way to manipulate integrator gain.

The potential for large gain carries with it a potential for instability. The inner product between a right eigenvector and the corresponding left eigenvector can vanish (or become vanishingly small) only when the Jordan normal form of \mathbf{M} is not diagonal. A non-diagonal Jordan form represents a bifurcation point: a point where a pair of real eigenvalues collide and split into a complex conjugate pair of eigenvalues. In order to achieve large gains, the brainstem-cerebellar system must operate near this bifurcation point.

Fig. 2 Phase planes as a function of PC–VU weights (ρ_2, ρ_1) for (a) a normal, and (b) an abnormal brainstem-cerebellar network. The Hopf curve, envelope, and $\lambda = -0.05\text{s}^{-1}$ curves divide the plane into regions characterized by the arrangement of the dominant eigenvalues. Insets A–G are cartoons of the locations of the eigenvalues in the complex plane for parameter values in the regions labelled with the corresponding letter. In Fig. 2(b) only the regions relevant to the CN simulations in Fig. 3(b–f) are labelled. The cycloidal CN is produced by toggling between two phase planes (see text); the phase plane shown is cycloidal left as described in Table 1



We explore this bifurcation by determining several boundary-defining curves in the phase plane for the system using differential geometry (Spivak 1999). Phase planes for the normal and abnormal networks are shown in Fig. 2(a), (b). In the network given by Eq. (5), feedback through the PCs ($\rho_1, \rho_2 \neq 0$) forms a rank-two perturbation of the system defined without feedback through the PCs ($\rho_1, \rho_2 = 0$). Due to this special structure the equation for the eigenvalues takes the following form:

$$\det(\mathbf{M} - \lambda \mathbf{I}) = D(\lambda) + P_1(\lambda)\rho_1 + P_2(\lambda)\rho_2 + Q(\lambda)\rho_1\rho_2 = 0 \tag{7}$$

where $D(\lambda)$, $P_i(\lambda)$, and $Q(\lambda)$ are polynomials. This result is known as the Aronszajn-Krein formula (Simon 1993).

Considering λ as a parameter, Eq. (7) defines a family of curves in the (ρ_2, ρ_1) plane representing the values of (ρ_2, ρ_1) for which λ is an eigenvalue. For instance, for the integrating mode, $\lambda = -0.05\text{s}^{-1}$ and we get the equation

$$D(-0.05) + P_1(-0.05)\rho_1 + P_2(-0.05)\rho_2 + Q(-0.05)\rho_1\rho_2 = 0$$

or equivalently

$$\rho_1 = -\frac{P_1(-0.05) + Q(-0.05)\rho_2}{D(-0.05) + P_2(-0.05)\rho_2}.$$

This curve represents the set of all points in the (ρ_2, ρ_1) plane for which $\lambda = -0.05\text{s}^{-1}$ is an eigenvalue of the model. Note that it may not be the dominant eigenvalue. In Fig. 2(a), (b) this $\lambda = -0.05\text{s}^{-1}$ curve, corresponding to normal, leaky integration with a time-constant of 20s, is shown in red dashed bold.

There is a second curve which contains information about the bifurcation points. The envelope of the family of constant eigenvalue curves is defined to be the curve that is tangent to each curve in the family (Spivak 1999). The envelope curve can be found as the simultaneous solution to

$$D(\lambda) + P_1(\lambda)\rho_1 + P_2(\lambda)\rho_2 + Q(\lambda)\rho_1\rho_2 = 0 \quad (8)$$

$$D'(\lambda) + P_1'(\lambda)\rho_1 + P_2'(\lambda)\rho_2 + Q'(\lambda)\rho_1\rho_2 = 0. \quad (9)$$

The above equations define a curve in the (ρ_2, ρ_1) plane that represents the values of (ρ_2, ρ_1) for which there is a bifurcation. This curve is smooth except for cusps at isolated points where the second derivative of Eq. (8) with respect to λ equals zero. The envelope curve is shown as the blue dotted curve in Fig. 2(a), (b). The 20s time-constant curve is tangent to the envelope at the point of maximum gain. Beyond this point integrator function becomes unstable.

We also define the Hopf curve (green dotted curve in Fig. 2(a), (b)) to be the locus of points where \mathbf{M} has a pair of purely imaginary eigenvalues. The Hopf curve originates from the point of tangency between the envelope and the zero eigenvalue curve. (The zero eigenvalue curve is not shown since at this scale it is indistinguishable from the -0.05s^{-1} eigenvalue curve.) The Hopf curve represents the boundary between decaying and unstable oscillation. It is given by the simultaneous solution to

$$\text{Re}(\det(\mathbf{M} - i\omega\mathbf{I})) = 0 \quad (10)$$

$$\text{Im}(\det(\mathbf{M} - i\omega\mathbf{I})) = 0. \quad (11)$$

When the parameters (ρ_2, ρ_1) are changed in such a way as to cross the Hopf curve the model undergoes a change in behavior, with an exponentially damped oscillation giving rise to an exponentially growing oscillation.

Finally we define the dominance curve (black solid curve in Fig. 2(a), (b)) to be the curve along which a real eigenvalue and a complex pair have equal real part. The dominance curve originates from a cusp in the envelope. When the parameters are changed in such a way as to cross the dominance curve a real eigenvalue

and a complex conjugate pair of eigenvalues exchange dominance.

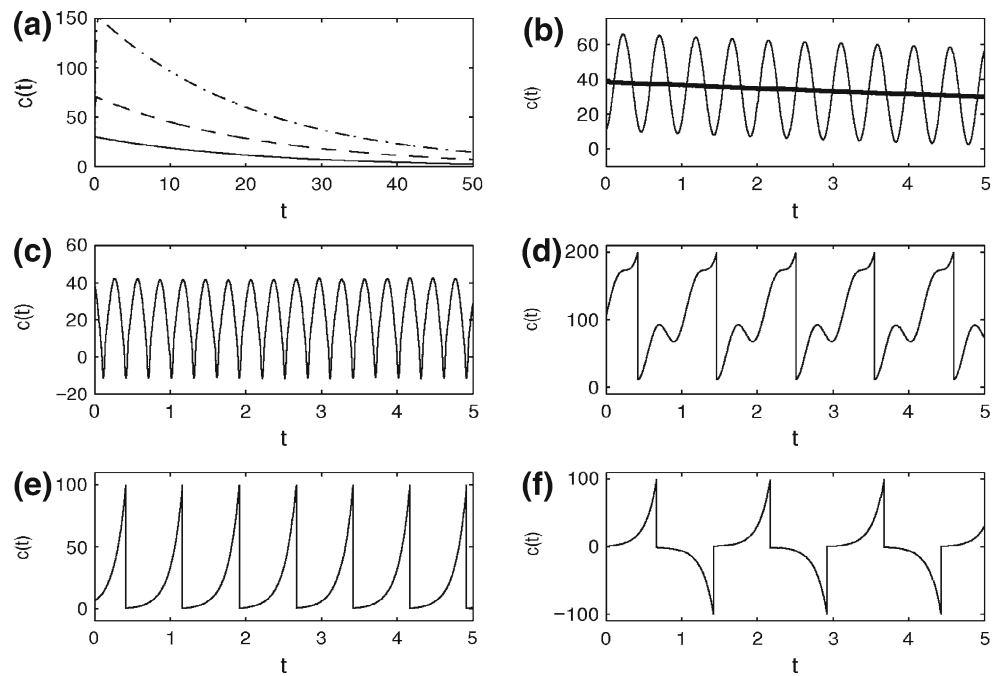
3 Results

Both networks behave as normal leaky integrators when gain is small. The networks are distinguished by their behavior as one moves up the constant eigenvalue curve and gain is increased. In the normal network (Fig. 2(a)) the 20s time-constant curve $\rho_1 = \frac{0.137+2.536\rho_2}{1+0.371\rho_2}$ crosses neither the Hopf nor the dominance curves. Thus, gain can be increased in the normal network without introducing sustained oscillation. Above the point of maximal gain (i.e. the point at which the 20s time-constant curve is tangent to the envelope), a previously subdominant real eigenvalue crosses the eigenvalue corresponding to a time-constant of 20s (the integrating mode), and the normal network behaves either as a stable integrator with time-constant greater than 20s, or as an unstable integrator.

In contrast, in the abnormal network (Fig. 2(b)), the constant eigenvalue curve crosses both the Hopf and the dominance curves at locations that correspond to relatively low values of gain. Thus, increasing the gain of the abnormal network beyond a certain threshold causes an exchange of dominance between the integrating mode and a complex conjugate pair of eigenvalues that results in sustained oscillation. Both the normal and abnormal networks can become unstable as gain is increased past the point of tangency of the constant eigenvalue curve and the envelope. The relationship in the model between high gain and both oscillation and instability is consistent with the observation that factors that increase oculomotor gain also exacerbate CN symptoms (Dell'Osso et al. 1974; Optican and Zee 1984; Dell'Osso and Daroff 1975; Yee et al. 1976).

In the normal network adjustments of the PC–VU weights within the normal operating regime produce high gains and arbitrarily long decays. In humans, integrator gain can be adaptively modified up or down by a factor of two at most (Tiliket et al. 1994). The middle circle in Fig. 2(a), at approximately $(\rho_2 = 0.96, \rho_1 = 1.89)$, gives an arbitrary medium gain of $g = 5.93$. The other two circles represent gains of slightly less than half this value, $g = 2.52$, attained for $(\rho_2 = 0.65, \rho_1 = 1.44)$, and slightly more than twice this value, $g = 12.9$, attained for $(\rho_2 = 1.09, \rho_1 = 2.07)$. The maximum gain point occurs at $(\rho_2 = 1.22, \rho_1 = 2.23)$. For reference the gain in the absence of Purkinje cells $(\rho_2 = 0, \rho_1 = 0)$ is $g = 0.91$. Normal network responses at these three gain levels and at a time constant of

Fig. 3 Simulating various forms of CN. **(a)** Response of the normal network to variations in (ρ_2, ρ_1) . **(b)** Sinusoidal pendular CN superimposed on normal leaky-integrator behavior. For reference, the normal integrating mode as it would appear by itself is depicted in bold. **(c)** Cycloidal CN. **(d)** Dual-jerk CN. **(e)** Unidirectional jerk CN. **(f)** Bidirectional jerk CN



20s are shown in Fig. 3(a). Similar gain adjustment is possible at virtually any time constant.

Note that, as the analysis suggests, as one moves up the gain curve the gain of the integrator depends more sensitively on the parameters, and one can produce rather substantial changes in the gain with fairly modest adjustments in the ρ values. Small movements away from the normal operating regime (portions of A and G near the dashed red line in Fig. 2(a)) can cause the dynamics of the normal network to become unstable (B, C, or D in Fig. 2(a)), oscillatory (F), or both (E). This triple-point characteristic enables the normal network to simulate some, but not all, types of CN. Jerk CN consists of eye movements of exponentially increasing velocity that are periodically interrupted by fast, resetting eye movements (Dell’Osso et al. 1972, 1974; Dell’Osso and Daroff 1975; Yee et al. 1976). PC–VU weight values with loci inside the envelope cusp can cause one or more positive, real eigenvalues, and produce the instability characteristic of jerk CN.

Pendular CN consists of oscillatory eye movements that are either quasi-sinusoidal or cycloidal, and that are superimposed on apparently normal integrator functioning (Dell’Osso et al. 1972, 1974; Dell’Osso and Daroff 1975; Yee et al. 1976). PC–VU weight values with loci outside the envelope cusp can result in a complex pair of dominant eigenvalues. These networks would display harmonic oscillation, but would not also exhibit neural integration. Because the exchange of dominance occurs on the envelope (and not on the dominance curve) in the normal network (Fig. 2(a)),

the integrating mode exchanges dominance with a real eigenvalue rather than a complex pair. At no point in the phase diagram does the integrating mode coexist with a sustained (real part near zero) oscillatory mode. Thus, the normal network could not be used to simulate pendular CN.

The integrating mode can coexist with a sustained oscillatory mode in the abnormal network (Fig. 2(b)), because the exchange of dominance occurs at low gain values outside the envelope cusp. Thus, the abnormal network offers richer pathology (Fig. 3(b–f)). An abnormal network with a real mode corresponding to a time constant of 20s and a complex mode with near-zero real part (A in Fig. 2(b)) would have normal integrator behavior upon which is superimposed stable oscillation (Fig. 3(b)). This case would correspond to quasi-sinusoidal, pendular CN that is independent of orbital position (Dell’Osso et al. 1974). Oscillations over a broad range of frequencies are possible, and changes in the VU–PC connectivity can change the frequency of pendular CN simulated by the model. For example, modest changes in the vector $\vec{w}_{1,2}$, detailed in Table 1, change the frequency of oscillation from 2.5Hz to 10Hz. We can simulate cycloidal pendular CN (Fig. 3(c)) by defining an arbitrary eye-position command level (here five) and switching between these \vec{w} vectors as the command crosses that level. Such switching between slightly different VU–PC connectivity patterns could occur in the actual brainstem-cerebellar network due to cut-off by some MVN/NPH neurons for commands in their off-directions (Stahl and Simpson

1995). Cut-off of an MVN/NPH neuron is equivalent to switching its output weight value to zero. Cut-off of subsets of MVN/NPH neurons effectively changes the configuration of VU–PC weights as a function of eye position, and could cause switching between the different forms of CN. Just as cut-off could cause the abnormal network to switch between oscillatory forms of CN at different frequencies, thus simulating cycloidal CN (Fig. 3(c)), it could also cause it to switch between oscillation and instability (not shown), thus simulating the position dependent transition from pendular to jerk CN observed in some patients (Dell’Osso et al. 1974; Dell’Osso and Daroff 1975).

An abnormal network with an unstable real mode and a complex mode with near-zero real part (B in Fig. 2(b)) would exhibit oscillation superimposed on instability. This case would correspond to dual-jerk CN (Optican and Zee 1984; Reccia et al. 1986). For simplicity, we simulate resetting eye movements by reinitializing the initial conditions when the amplitude exceeds a predetermined threshold. Figure 3(d) shows simulated dual-jerk CN in which resetting eye movements undershoot the midline. One or more real, unstable modes with no complex modes (C in Fig. 2(b)) would correspond to jerk CN. Figure 3(e) shows simulated unidirectional jerk CN (running away in only one direction), in which the fast, resetting eye movements undershoot the midline. Figure 3(f) shows simulated bidirectional jerk CN (alternately running away in either direction), in which the resetting eye movements overshoot the midline. Using undershoot or overshoot of resetting saccades to simulate unidirectional or bidirectional jerk CN was a strategy also adopted in a previous modeling study (Optican and Zee 1984). Note that the changes in PC–VU weights that bring about all the different forms of CN in the abnormal network are only about one-tenth the size of the changes that adjust gain over the physiological range in the normal network (compare the distances between the dots in Figs. 2(a) and 2(b), and note axis scales).

4 Discussion

Evidence indicates that oculomotor neural integration results from positive feedback among the neurons that compose the integrator network, and that this feedback is tuned by adaptive cerebellar mechanisms (Zee et al. 1981; Robinson 1989; Tiliket et al. 1994). Tuning of positive feedback weights is a sensitive process because of the potential for instability. Our analysis shows that there is also a potential for oscillation. As shown in Anastasio and Gad (2007), a plausible,

stochastic learning rule is able to adapt the weights of the brainstem-cerebellar model to achieve independent adjustment of integrator time constant and gain over broad ranges, while avoiding both instability and oscillation. Our analysis suggests that independent adjustment of integrator time constant and gain in the real system should be possible, provided that the connectivity and adaptive capability of the cerebellum are normal, but that an abnormal cerebellum cannot move integrator time constant and/or gain into operational ranges without also introducing oscillation and/or instability.

Our model is capable of simulating the full range of waveform types observed in CN (Dell’Osso et al. 1972, 1974; Optican and Zee 1984; Dell’Osso and Daroff 1975; Yee et al. 1976; Reccia et al. 1986) and requires only small changes from normal operation in a network that achieves its desired characteristics (high gain and long time constant) by operating near a triple point of its phase space. It suggests that CN could result from an abnormal pattern of connections from brainstem neurons to cerebellar Purkinje cells, which could result, in turn, from misdirection of developing axons or limitations of synaptic plasticity. Recent results support this suggestion. CN in humans has been associated with mutations in the *FRMD7* gene, which encodes a protein similar to proteins that modulate the length and degree of branching of developing axons (Tarpey et al. 2006). Mutant mice deficient in the glutamate receptor γ_2 subunit, which have limited plasticity of synapses onto Purkinje cells, also have oscillations of about 10Hz in Purkinje cell responses and eye movements that resemble pendular CN (Yoshida et al. 2004).

Acknowledgements We thank Joseph Malpeli and Gregory Stanton for comments on the manuscript. This research was supported in part by NSF grant DMS0354462 to JCB.

References

- Akman, O., Broomhead, D., Abadi, R., & Clement, R. (2005). Eye movement instabilities and nystagmus can be predicted by a nonlinear dynamics model of the saccadic system. *Mathematical Biosciences*, *51*, 661–694.
- Anastasio, T. J., & Gad, Y. P. (2007). Sparse cerebellar innervation can morph the dynamics of a model oculomotor neural integrator. *Journal of Computational Neuroscience*, *22*, 239–254.
- Babalian, A. L., & Vidal, P. P. (2000). Floccular modulation of vestibuloocular pathways and cerebellum-related plasticity: An *in vitro* whole brain study. *Journal of Neurophysiology*, *84*, 2514–2528.
- Büttner-Ennever, J. A. (1988). *Neuroanatomy of the oculomotor system*. Amsterdam: Elsevier.

- Cannon, S. C., & Robinson, D. A. (1987). Loss of the neural integrator of the oculomotor system from brain stem lesions in monkey. *Journal of Neurophysiology*, *57*, 1383–1409.
- Chelazzi, L., Ghirardi, M., Rossi, F., Strata, P., & Tempia, F. (1990). Spontaneous saccades and gaze holding ability in the pigmented rat. II. Effects of localized cerebellar lesions. *European Journal of Neuroscience*, *2*, 1085–1094.
- Dell'Osso, L. F. (1982). *Congenital nystagmus—basic aspects* (pp. 129–138). Oxford: Pergamon.
- Dell'Osso, L. F., & Daroff, R. B. (1975). Congenital nystagmus waveforms and foveation strategy. *Documenta Ophthalmologica*, *39*, 155–182.
- Dell'Osso, L. F., Flynn, J. T., & Daroff, R. B. (1974). Hereditary congenital nystagmus. *Archives of Ophthalmology*, *92*, 366–374.
- Dell'Osso, L. F., Gauthier, G., Liberman, G., & Stark, L. (1972). Eye movement recordings as a diagnostic tool in a case of congenital nystagmus. *American Journal of Optometry and Archives of American Academy of Optometry*, *49*, 3–13.
- Embre, M., & Trefethen, L. N. (2001). Generalizing eigenvalue theorems to pseudospectra theorems. *SIAM Journal of Scientific Computing*, *23*(2), 583–590.
- Harris, C. M., & Berry, D. L. (2006). A distal model of congenital nystagmus as nonlinear adaptive oscillations. *Nonlinear Dynamics*, *44*, 367–380.
- Jacobs, J. B., & Dell'Osso, L. F. (2004). Congenital nystagmus: Hypotheses for its genesis and complex waveforms within a behavioral ocular motor system model. *Journal of Vision*, *4*, 604–625.
- Maybodi, M. (2003). Infantile-onset nystagmus. *Current Opinion in Ophthalmology*, *14*, 276–285.
- Optican, L. M., & Zee, D. S. (1984). A hypothetical explanation of congenital nystagmus. *Biological Cybernetics*, *50*, 119–134.
- Reccia, R., Roberti, G., Russo, P., & Segre, G. (1986). Spectral analysis of dual-jerk waveforms in congenital nystagmus. *Biological Cybernetics*, *55*, 211–217.
- Robinson, D. A. (1989). Integrating with neurons. *Annual Review of Neuroscience*, *12*, 33–45.
- Simon, B. (1993). *Spectral analysis of rank one perturbations and applications*. Lectures given at the Vancouver Summer School in Mathematical Physics.
- Spivak, M. (1999). *Differential geometry* (vol. III, 3rd ed.). Houston: Publish or Perish.
- Stahl, J. S., & Simpson, J. I. (1995). Dynamics of rabbit vestibular nucleus neurons and the influence of the flocculus. *Journal of Neurophysiology*, *73*, 1396–1413.
- Tarpey, P., Thomas, S., et al. (2006). Mutations in *FRMD7*, a newly identified member of the FERM family, cause X-linked idiopathic congenital nystagmus. *Nature Genetics*, *38*, 1242–1244.
- Tiliket, C., Shelhamer, M., Roberts, D., & Zee, D. S. (1994). Short term vestibulo-ocular reflex adaptation in humans. I. Effect on the ocular motor velocity-to-position neural integrator. *Experimental Brain Research*, *100*, 316–327.
- Trefethen, L. N. (1997). Pseudospectra of linear operators. *SIAM Review*, *39*, 383–406.
- Yee, R. D., Wong, E. K., Baloh, R. W., & Honrubia, V. (1976). A study of congenital nystagmus waveforms. *Neurology*, *26*, 326–333.
- Yoshida, T., Katoh, A., Ohtsuki, G., Mishina, M., & Hirano, T. (2004). Oscillating purkinje neuron activity causing involuntary eye movement in a mutant mouse deficient in the glutamate receptor γ_2 subunit. *Journal of Neuroscience*, *24*, 2440–2448.
- Zee, S., Yamazaki, A., Butler, P. H., & Gücer, G. (1981). Effects of ablation of flocculus and paraflocculus on eye movements in primate. *Journal of Neurophysiology*, *46*, 878–899.